SCIENCE CHINA
Chemistry

• REVIEWS •
• SPECIAL ISSUE • Recent Research Progress of Biomedical Polymers

April 2014 Vol.57 No.4: 522–539
doi: 10.1007/s11426-014-5064-4

Biological applications of carbon dots

WANG Wei, CHENG Lu & LIU WenGuang*

Tianjin Key Laboratory of Composite and Functional Materials, School of Materials Science and Engineering, Tianjin University, Tianjin 300072, China

Received October 23, 2013; accepted November 23, 2013; published online March 6, 2014

Carbon dots (C-dots), since their first discovery in 2004 by Scrivens *et al.* during purification of single-walled carbon nanotubes, have gradually become a rising star in the fluorescent nanoparticles family, due to their strong fluorescence, resistance to photobleaching, low toxicity, along with their abundant and inexpensive nature. In the past decade, the procedures for preparing C-dots have become increasingly versatile and facile, and their applications are being extended to a growing number of fields. In this review, we focused on introducing the biological applications of C-dots, hoping to expedite their translation to the clinic.

carbon dots, fluorescence, biological application

1 Introduction

Carbon dots (C-dots) were discovered accidentally in 2004 by researchers in the process of purifying single-walled carbon nanotubes (SWCNTs) fabricated by arc-discharge methods. This carbonaceous material with size-dependent fluorescent properties was observed through separation of SWCNTs from the crude suspension by gel electrophoresis. The basic properties of this then-unknown fluorescent nanomaterial, which was considered as "promise to be interesting nanomaterials in their own right", were further characterized [1]. Since their discovery, these materials have come to be known as carbon dots or carbon nanodots, and intensive studies were carried out on their synthetic routes, photophysical behavior and novel applications [1–5].

During the past few years, many methods have been developed to prepare C-dots, including laser ablation, arc-discharge, electrochemical oxidation, acid dehydration, microwave heating, combustion/thermal and supported routes, etc [2, 3, 6]. These methods can be classified into two categories: top-down and bottom-up methods [3]. The top-down approaches are primarily based on the post treatment of nanocarbon exfoliated from various larger carbon structures, such as carbon nanotubes, graphene, nanodiamond and commercial activated carbon [2, 3, 7–9]. The bottom-up approaches generally involve the carbonization of suitable precursors, such as glucose, sucrose, glycerol, citric acid, orange juice, candle soot or natural-gas burner, carbohydrates, chitosan gel, bovine serum albumin, bombyxmori silk and dextrin [10–19]. In our previous work, we have prepared strong luminescent C-dots by one-step microwave assisted pyrolysis of glycerol, citric acid, acrylic acid as well as phytic acid [18, 20–23].

C-dots are composed of carbon (C), oxygen (O), nitrogen (N), hydrogen (H) and some doped elements [22, 24–26]. The elemental analysis of typical C-dots was: C, 53.93%; H, 2.56%; N, 1.30%; and O, 40.33% [1]. Nuclear magnetic resonance (NMR) measurements by Wang *et al.* showed that carbon atoms in C-dots were sp^2 hybridized with unsaturated sp^3 carbon atoms, indicating that C-dots are conjugated systems [15]. Ray *et al.* [27] concluded that candle soot derived C-dots consisted of a nanocrystalline core of graphitic sp^2 carbon atoms with peripheral carboxylic/

*Corresponding author (email: wgliu@tju.edu.cn)

carbonyl functionalization. However, some C-dots showed poor crystallization (the C-dots prepared by controlled carbonization of sucrose, for example) [28]. In fact, X-ray diffraction pattern of C-dots in another research displayed a broad diffraction peak at $2\theta = 20.8°$, indicating their amorphous nature [29].

Being competitive to other fluorescent counterparts, C-dots have shown conspicuous photoluminescent (PL) properties with emission tunability and photostability. Yet the mechanisms of their luminescence have not been fully understood. Radiative recombination of the carbon nanoparticle surface-confined electrons and holes may be responsible for the observed bright fluorescence. The electrons and holes were likely generated from efficient photoinduced charge separations in the C-dots. Interestingly, the requirement of surface passivation for PL was apparently shared by a series of C-dots and QDs, for which the widely accepted mechanism for luminescence was the radiative recombination of excitons [30]. It was also proposed that the emission originated from deep trap on the surface of C-dots [31]; an alternative proposal, however, lied in the quantum confinement effect on C-dots, a similar mechanism derived from that of II-VI (or III-V) semiconductor nanoparticles [32]. Recently, Lai [33] and Eda [34] *et al.* speculated that the isolated sp^2 clusters in carbon-oxygen nanomaterials with large gaps which could lead to radiative recombination were responsible for the blue luminescence. In addition, the multicolor PL arises not only from a distribution of different emissive trap sites, but also from C-dots of different sizes, which will be discussed later [2]. Kang *et al.* [35] presented definitive evidence for luminescence arising from quantum-confinement effects and size-dependent optical properties of C-dots prepared according to alkali-assisted electrochemical method.

Besides their unique intrinsic properties, C-dots are easily imparted with excellent surface tailorability owing to the abundant reactive functional groups on the surface. Actually, C-dots are versatile and have been used in a wide range of fields, such as bioimaging, photocatalysis, fluorescent ink, sensing, lasers, LED, polymerizable C-dots, and energy conversion/storage devices [7, 18, 30, 36–42].

Several reviews have been published focusing on the preparation methods and properties of C-dots [3] or emphasizing their potential applications, especially in photocatalysis, energy conversion and optoelectronics [2]. More recently, achievements in functional surface engineering of C-dots, aiming at improving quantum yield, stability and lowering cytotoxicity for better biomedical utilization, were reviewed [43]. Yet, a systematic summary of their applications specifically in biological field has not been documented in literature. Herein we describe the recent advances in the research on C-dots, focusing on their biological applications.

2 Advantages in bioapplications

2.1 Fluorescent properties

The most fascinating feature of C-dots is their luminescence, including photoluminescence (PL), chemiluminiscence (CL) and electrochemiluminescence (ECL). A significant PL property of C-dots is the excitation-dependence of emission wavelength and intensity. In general, C-dots show strong optical absorption in the UV region, with a tail extending out into the visible range (Figure 1). The polyethyleneimine (PEI) passivated C-dots prepared by our group exhibited blue, green and red luminescence under ultraviolet (330–385 nm), blue (460–495 nm) and green (530–550 nm) light excitation, respectively, and the PL intensity decreased remarkably with longer shifted excitation wavelengths (Figure 2) [21]. Although the full width at half maximum (FWHM) was relatively low [44, 45], their emission, when compared

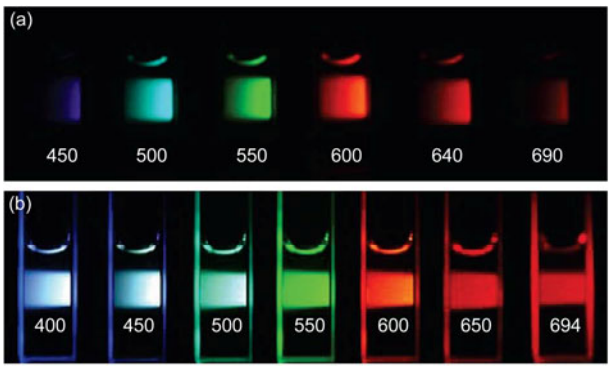

Figure 1 Aqueous solution of the PEG 1500N-attached C-dots (a) excited at 400 nm and photographed through band-pass filters of different wavelengths as indicated, and (b) excited at the indicated wavelengths and photographed directly [31].

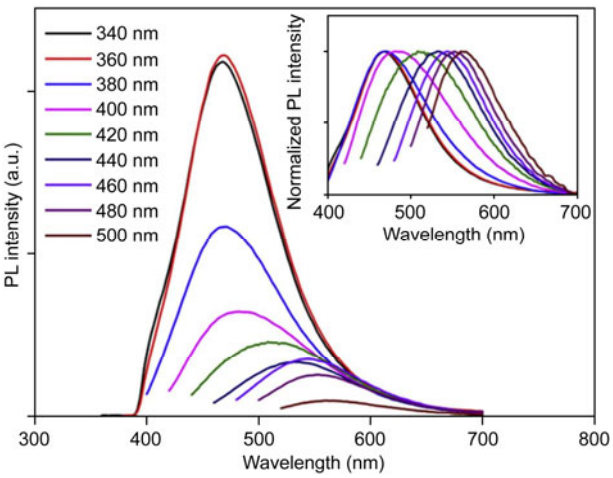

Figure 2 Photoluminescence emission spectra of CD-PEI (progressively longer excitation wavelengths from 340 to 500 nm with a 20 nm increment) and the emission spectral intensities are normalized in the inset [21].

with that of semiconductor nanoparticles, however, was commonly broad, which may be attributed to the lack of size uniformity [33].

C-dots are considered as a class of zero-dimensional carbon nanomaterials with a size below 10 nm, which can be cleared from the body by renal excretion [8]. The PL properties varied sensitively with C-dots size and a red shift was observed with increase in particle size. Kang's research showed that the bright blue, green, yellow, and red PL of C-dots illuminated by UV light was strong enough to be seen with naked eye. Small C-dots (1.2 nm) gave UV light emission, while medium sized C-dots (1.5–3 nm) provided visible light emission (400–700 nm), and large C-dots (3.8 nm, center) led to near-infrared emission [35]. The C-dots produced by electrochemical oxidation of graphite were selected into (1.9 ± 0.3) and (3.2 ± 0.5) nm fractions by MW cut-off membranes, showing size-dependent but excitation-independent emissions [46]. Recently, Vinci *et al.* [47] reported that the C-dots derived from graphite nanofibers existed in a complex mixture, which could be reduced significantly by high resolution anion-exchange high-performance liquid chromatography (AE-HPLC) fractionation. It was particularly interesting that the fractionated C-dots components did not display wavelength-dependent emission, which was considered as a characteristic attributed as an intrinsic property of luminescent C-dots.

Owing to their PL feature, C-dots have been widely studied for optical bioimaging. However, most fluorescent imaging studies were carried out under UV or visible excitation. Interestingly, C-dots can exhibit PL emission in the near-infrared (NIR) spectral region under longer wavelength excitation. Compared to conventional measurements in UV-Visible region, spectrofluorimetry within the therapeutic window of 700–1200 nm has many advantages, such as lower levels of background interference and deeper penetration into living tissues. NIR PL holds great promise for *in vivo* uses at significant depth in biological media and the development of noninvasive diagnostic techniques [48]. The corresponding visible emissions of C-dots covering blue-to-red wavelength range can be obtained from the same sample under UV and visible excitations. The NIR PL emissions can be obtained under different NIR excitations (700, 750, 800, and 850 nm) [49]. It should be noted that such NIR PL emissions excited by NIR excitation is particularly significant and useful for bio-nanotechnology because of the transparency of body tissues in the NIR "water window" [49].

Ionic strength and pH values are known to affect the fluorescent properties of different molecules and nanoparticles. The dependence of the C-dots PL intensity on pH value was reported in a few studies. For example, Zhao *et al.* [46] found the intensity decreased when the pH value of the solution was higher or lower than 4.5, but could be totally recovered when the pH value was adjusted back to this optimal value. At the same time, a slight shift of the emission peak was found with variation of pH value. Generally speaking, C-dots are chemical inertness, having the ability to resist acids, bases and high ionic strength environments. They can also maintain photostability in most common organic solvents and in complex systems [7, 10, 24]. The photostability of C-dots was compared with fluorescein by exposing both solutions under a high-brightness cold light (350 W). The fluorescence of fluorescein decreased by 60% in 2 h, and almost disappeared after light exposure for 6 h, while no photo bleaching of C-dots was observed even after 24 h (Figure 3) [8]. Actually, it was reported that the fluorescence and the quantum yield (QY) of C-dots can stay at least several months with negligible decrease [13, 49].

Luminescence decays from laser ablation-produced C-dots, excited at 407 nm, showed multi-expotential PL decays with average excited-state life times of 5 ns for emission at 450 nm and 4.4 ns for emission at 640 nm [31]. Microwave-synthesized C-dots were found to have a mean PL lifetime of (8.7 ± 0.05) ns [44], which was much longer than most reported C-dots [50]. Recently, pure organic room temperature phosphorescence (RTP) on a C-dots-PVA composite film was observed by Deng *et al.* [51]. The phosphorescent emission peak was located at 500 nm with a very long lifetime of 380 ms under the 325 nm excitation. The phosphorescence is attributed to C=O bonds on the surface of C-dots, and the PVA matrix effectively protects their triplet states from being quenched by intramolecular motions and oxygen.

2.2 Quantum yield

Quantum yield (QY) is an important parameter for practical application. The QY of C-dots varies with the fabrication and separation methods and the surface chemistry involved. C-dots prepared by Sun *et al.* via laser ablation method were observed to have QYs ranging from 4% to over 10% [30]. Later on, Yang's group [52] presented the QY of C-dots synthesized by a well-refined hydrothermal method reached up to 80% under the optimized reaction conditions, the highest QY ever reported for C-dots.

The effectiveness of surface passivation could affect the

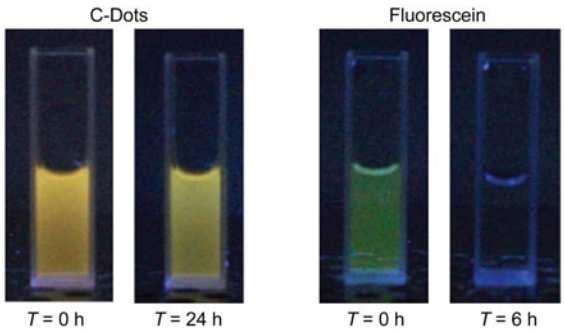

Figure 3 Photos of C-dots and fluorescein under UV light before and after being exposed to the high-brightness cold light source [8].

optical performance of C-dots in a dramatic fashion [5, 33, 53, 54]. "Naked" C-dots without surface functionalization were shown to exhibit colorful fluorescence emissions but with generally low to very low QYs (lower than 10% or even 1%) [27, 41], but the passivation of the C-dots with polymers or other organic molecules can increase the QYs dramatically [55]. C-dots were solvothermally synthesized in water-glycol medium by using glucose as carbon source. PEI modification led to 300-fold enhancement in fluorescence intensity and red shift in emission wavelength [8]. The requirement for surface passivation was little understood, but appeared to be linked to the synthetic method [35, 56]. C-dots produced from MWCNTs by an electrochemical oxidation method exhibited blue PL (when excited at 365 nm). No further passivation step was required for PL to occur [45]. In Hu's study [57], PL occurred when C-dots formed directly in the presence of PEG200Da were excited at 420 nm. However, no PL occurred when C-dots were formed in water with only methyl and a few carboxylic moieties present on the surface. Only minimal PL was observed even after many more carboxylic moieties were produced on the surface by oxidation in perchloric acid. Interestingly, subsequent passivation of these C-dots by incubation in PEG200Da led to the production of strong PL emission. These results demonstrated how the surface chemistry could significantly affect the PL properties of C-dots and QYs. On the other hand, the surface passivation molecules on C-dots could allow for their conjugation with bioactive species for specific applications.

C-dots doped with other elements or inorganic salts were fabricated to achieve much higher QYs. In our previous research, C-dots were synthesized by one-step microwave-assisted pyrolysis of citric acid in the presence of various amines including diethylamine, triethylamine and 1,4-butanediamine. The QY of 30.2% was obtained without additional passivation. In this case, the amine molecules played dual roles as N-doping precursors and surface passivation agents for the C-dots, both improving the PL performance [20]. Sun *et al.* [25, 26] doped the C-dots surface with inorganic salts (ZnO and ZnS). The resulting C-dots exhibited much brighter fluorescence, with the observed QY up to 50%, than those from the corresponding C-dots without doping. These new C-dots were competitive to the commercially available CdSe/ZnS dots.

2.3 Cytotoxicity

The available toxicity evaluation results suggest that C-dots are generally nontoxic or at least no more toxic than the selected polymeric species used as surface passivation agents in C-dots [3–5]. In our research, C-dots passivated by PEI25k showed much less cytotoxicity than the PEI control at the same concentrations in COS-7 cells and HepG2 cells [21]. Whereas, notable cytotoxicity of C-dots could only be detected at higher concentrations, much beyond what are required for optical cell imaging under a conventional fluorescence microscope [3, 5]. A number of other studies collectively concluded that C-dots were of no or low toxicity to various cell lines [5]. These parallel comparative studies revealed that the relative toxicity of three nanomaterials in their native forms was in the order: Cd/Te QDs >> Au nanoparticles > C-dots, with IC_{50} values for normal NIH/3T3 cells as 0.98, 62, and 250 μg/mL, respectively [58].

Furthermore, *in vivo* biodistribution and toxicology of C-dots via intravenous injection in mice were studied using a radiolabeling method. No obvious toxic effects of C-dots to the treated mice were observed in blood tests and histological analysis [8]. Some C-dots were found in liver, spleen, and kidneys, but the levels of accumulation were generally low. Serum biochemical parameters such as hepatic and renal toxicity indicators were still at normal levels. C-dots post-administration into mice (injection via the tail vein) were cleared via renal excretion within about 24 h. In addition, C-dots did not lead to any clinical symptoms in the mice during the observation period of up to 28 days post-administration [26]. Tao *et al.* [8] investigated the *in vivo* toxicology of C-dots in female Balb/c mice for over 90 days. Neither death nor significant body weight change was observed in the treated group of mice, and no obvious signs of toxic effects from C-dots were observed at the injected dosage of 20 mg/kg (Figure 4). In a more recent *in vivo* study, C-dots were prepared using the raw soot as carbon source by nitric acid oxidation method and were passivated with PEG. Mice or rats were intravenously exposed to C-dots through tail injection. The toxicity of C-dots was then systematically evaluated via acute toxicity, subacute toxicity, and genotoxicity experiments (including mouse bone marrow micronuclear test and Salmonella typhimurium mutagenicity test). No significant toxic effect and no abnormality or lesion was observed in the organs of the animals. The results showed that the fluorescent C-dots did not exert any significant toxic effect on rats and mice. The C-dots did not exhibit any gene toxicity, either [59]. Near-infrared fluorescent C-dots were fabricated by coupling the nanoparticles with the near-infrared dye ZW800, to track their *in vivo* fates and the effect of tumor uptake after three injection routes: intravenous, subcutaneous, and intramuscular, respectively. C-dots could be efficiently and rapidly excreted from the body after all three injection routes. The clearance rates of C-dots were ranked as intravenous > intramuscular > subcutaneous. The particles had relatively low retention in the reticuloendothelial system and showed high tumor-to-background contrast. Furthermore, different injection routes resulted in different blood clearance patterns and tumor uptakes of C-dots. The C-dot/ZW800 conjugate underwent rapid renal clearance, yet effective passive tumor targeting [60]. The conclusion based on currently available toxicity data was that the intrinsic configuration of C-dots was nontoxic *in vitro* and *in*

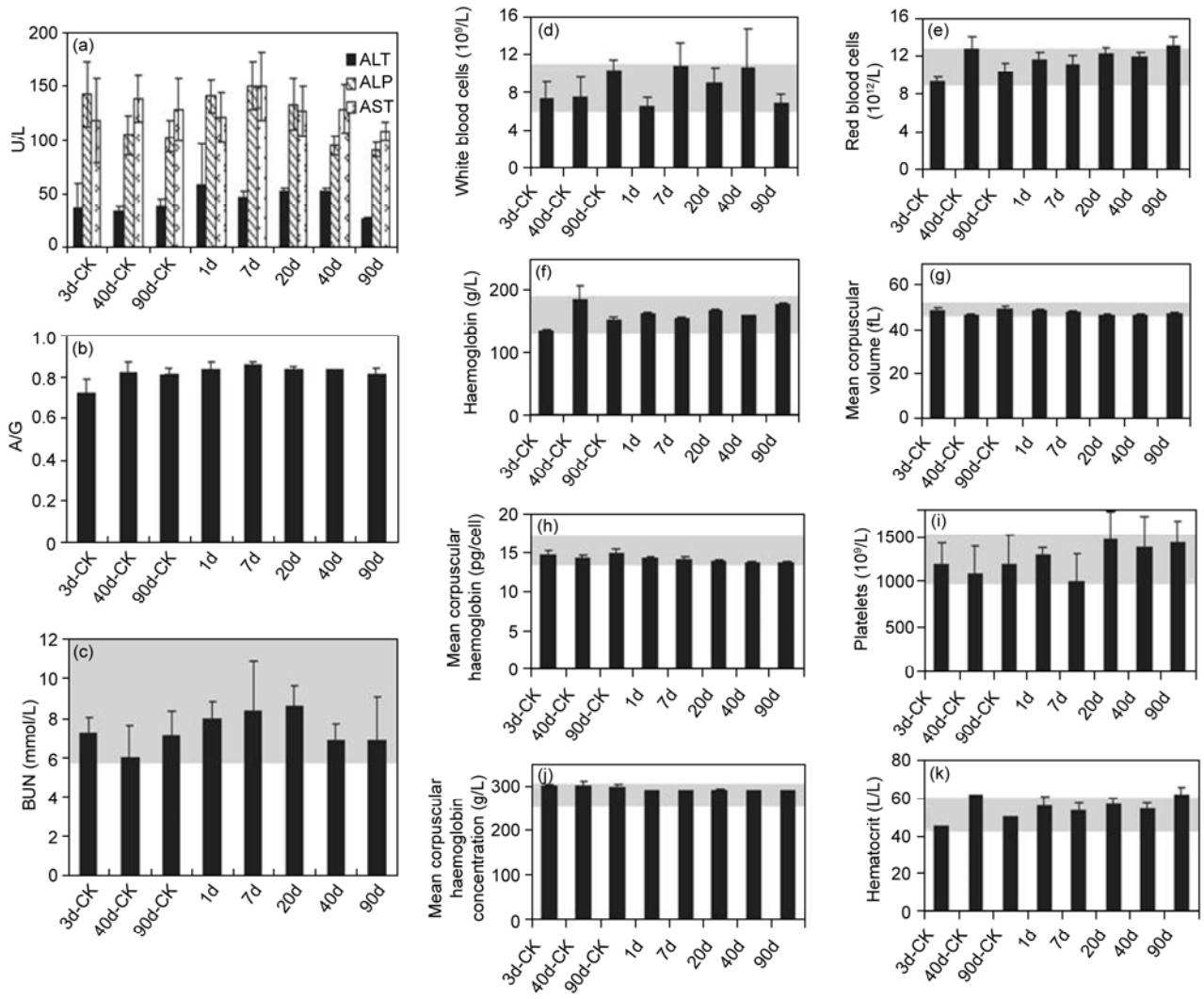

Figure 4 Blood biochemistry and hematology data of female Balb/c mice treated with C-dots-M at the dose of 20 mg/kg at 1, 7, 20, 40, and 90 days p.i. Age-matching untreated mice were sacrificed at 3, 40, and 90 day p.i. as controls (3d-CK, 40d-CK, and 90d-CK, respectively). (a) Alanine aminotransferase (ALT), aspartate aminotransferase (AST), and alkaline phosphatase (ALP) levels in the blood at various time points after C-dots-M treatment. (b) Time-course albumin/globin ratios. Blood chemistry data suggested no hepatic disorder induced by the C-dots treatment. (c) Blood urea nitrogen (BUN) over time. Time-course changes of white blood cells (d), red blood cells (e), hemoglobin (f), mean corpuscular volume (g), meancorpuscular hemoglobin (h), platelets (i), mean corpuscular hemoglobin concentration (j), and hematocrit (k) from control mice and C-dots-M-treated mice. Statistics were based on 5 mice per data point. Gray areas in the figures show the normal reference ranges of hematology data of female Balb/c mice [8].

vivo. Therefore, when considering toxicity issues of C-dots for specific bioapplications, the emphasis should be put on the selection of appropriate nontoxic molecules or species for C-dots surface functionalization, as their toxicity profiles may dictate how the resulting C-dots will behave.

2.4 Comparison with other fluorescent nanoparticles

C-dots have already demonstrated their feasibility in a variety of applications because they display PL properties reminiscent of those of QDs. The optical imaging performance of C-dots was evaluated in reference to that of the commercially supplied CdSe/ZnS QDs. C-dots show similar photophysical performance and photochemical stability compared with already commercialized QDs [26]. In addition, photoluminescent C-dots are superior in terms of chemical inertness, large two-photon excitation cross-sections, non-blink, easy functionalization, high resistance to photobleaching, low cytotoxicity, and excellent biocompatibility [61]. As widely acknowledged, however, a major issue for the QDs containing heavy metals is their toxicity. Existing data suggest that these QDs are toxic to vertebrate systems at relatively low concentrations, with possible accumulation in organs and tissues. Recently, it was reported that QDs could induce acute toxicity and prothrombotic effect in mice [59]. C-dots have proved to be a valuable tool to overcome the toxicity issues arising from the use of cadmium core based QDs. A toxicity assay of these new nanoparticles indicated that unlike the traditional cadmium based QDs and nanotubes, the accumulation level of C-dots in the liver was very

low [37, 62].

Another carbon-based nanomaterial with similar size and surface functionality to the C-dots is nanodiamond, which has been used in cell bioimaging, too [63]. Nanodiamonds are typically made from milling microdiamonds, chemical vapor deposition (CVD), shockwave, or detonation processes. They generally consist of about 98% carbon with residual hydrogen, oxygen, and nitrogen, possess a sp^3 hybridized core, and have small amounts of graphitic carbon on the surface. Unlike nanodiamonds, C-dots not only have greater sp^2 character, which is symbolic of nanocrystalline graphite, but also contain lower amounts of carbon with higher oxygen contents [3]. C-dots with tunable photoluminescence could be synthesized via one-pot hydrothermal oxidation of nanodiamond and subsequently utilized for cell imaging applications. Cell morphology observation and cell viability measurement demonstrated the good biocompatibility of C-dots for bioimaging applications [64].

3 Biological applications

3.1 Bioimaging and biolabeling

QDs such as CdSe and related core-shell nanoparticles have been used in optical imaging *in vitro* and *in vivo*. However, they have imposed serious health and environmental concerns due to the existence of heavy metals in such QDs. As a biocompatible alternative to QDs, C-dots have been demonstrated for successful uses in optical bioimaging applications, taking advantage of their visible excitation and emission wavelengths, fluorescence brightness at the individual dot level [5], high photostability, and low toxicity as revealed by both *in vitro* and *in vivo* evaluations.

In our previous study, C-dots were synthesized by one-step microwave assisted pyrolysis of glycerol in the presence of TTDDA. The formation and surface passivation of C-dots were accomplished simultaneously. In addition to the strong PL intensity and multicolor emissions, C-dots also demonstrated properties of rich hydrophilic groups, good solvent dispersibility, high photostability and low cytotoxicity. Cellular internalization of C-dots was observed by multicolor photoluminescence on confocal microscopy or even common fluorescence microscopy (Figure 5) [22]. A number of other studies were conducted using fluorescence by various C-dots in cell bioimaging of different cell lines [14, 65, 66], including Caco-2 cells [5], Ehrlich ascites carcinoma cells (EAC) from mice [27], pig kidney cell line (LLC-PK1 cells) [67], murine P19 progenitor cells [68] and MG-63 cells [69]. The cell imaging results suggested that C-dots taken up by cells were mostly localized in the cytoplasm. Wang *et al.* [61] incubated silica-encapsulated C-dots with BGC823 cells for 24 h, and observed fluorescence in the cytoplasmic area due to the expected penetration of the dots into the cells but not into the nuclei. Yang *et al.* [70] synthesized C-dots by hydrothermal carbonization of chitosan. The fluorescent dots were observed only inside the membrane and cytoplasmic area of A549 cells, with much weaker signals in the cell nucleus region. However, C-dots were distributed into cell nucleus in several studies. Ray *et al.* [27] found the whole EAC cells could be lighted to bright blue-green under UV excitation and yellow under blue excitation after the incubation with C-dots for 30 min, while the cytoplasm was brighter than the nucleus (though the nucleus was still brighter than that in the control cells). Chandra *et al.* [71] reported that C-dots tagged with organic molecules (α-naphthylamine, fluorescein, and rhodamine B) were distributed into the whole human red blood corpuscles (RBC), as suggested by results from confocal microscopy. More evaluations on C-dots for potential applications such as fluorescence labeling of cells, high-resolution and/or high-sensitivity cellular imaging may be expected to determine more precisely the intracellular distribution of the C-dots.

Recently, the application of C-dots for real time bioimaging of target specific delivery of hyaluronic acid (HA) derivatives was reported. PEG-diamine-capped C-dots were synthesized by the pyrolysis of citric acid in a hot solvent. The synthesized C-dots showed strong fluorescence under UV excitation, with emission properties depending on the excitation wavelength. HA/C-dots conjugates were synthesized by amidation reaction between amino groups of C-dots and carboxylic groups of HA (Figure 6). C-dots and HA/C-dots conjugates showed negligible cytotoxicity. According to *in vitro* bioimaging, HA/C-dots conjugate was

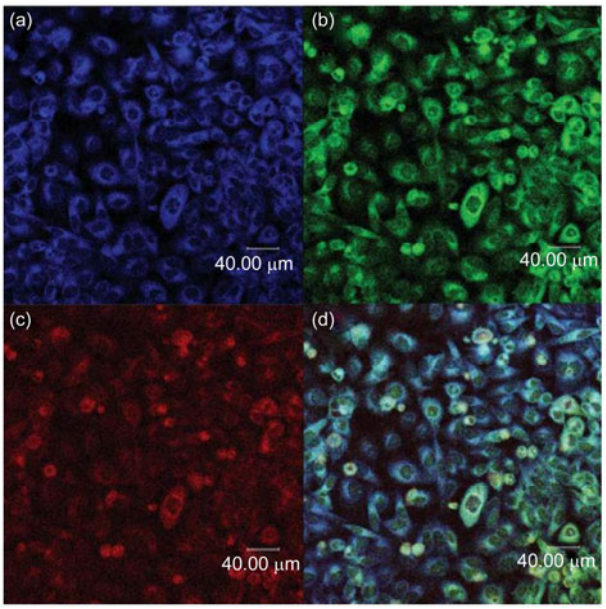

Figure 5 Laser scanning confocal microscopy images of C-dots labeled HepG-2 cells. The samples were (a) excited at 405 nm; (b) excited at 488 nm; (c) excited at 543 nm; (d) an overlay of (a), (b) and (c) [22].

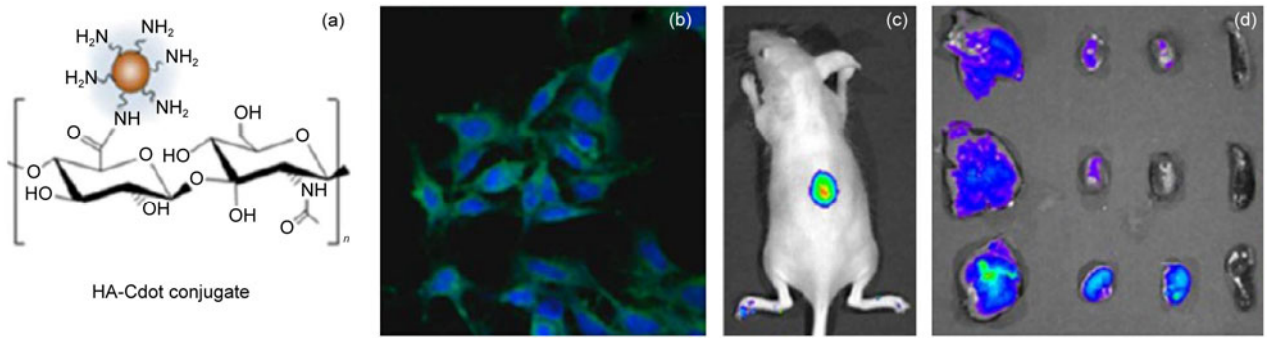

Figure 6 (a) Schematic illustration of HA-Cdots; (b) confocal laser scanning microscopic images of B16F1 cells for 24 h with HA-Cdots. Scale bar indicates 30 μm; (c) HA-Cdots conjugates after subcutaneous injection to Balb/c mice; (d) fluorescence images of dissected livers, kidneys, and spleens 4 h after tail-vein injections of Cdots or HA-Cdots conjugates [72].

target-specifically delivered to B16F1 cells with HA receptors, showing different fluorescence colors depending on the excitation wavelength. In addition, *in vivo* real-time bioimaging of C-dots and HA/C-dots conjugates revealed the target-specific delivery of HA/C-dots conjugates to the liver with HA receptors such as HARE and CD44 [72]. A more recent study demonstrated that the C-dots could influence DNA conformation, such as right-handed B-DNA to left-handed Z-DNA under physiological salt conditions, with sequence and conformation selectivity. The results showed that positively charged spermine-functionalized C-dots could induce DNA B-Z transition under physiological condition (PBS, pH 7.2) with sequence selectivity as shown in Figure 7. Moreover, their studies indicated that C-dots would bind to DNA major groove with GC preference [29]. We expect that C-dots can be employed to different cells and chemical or biological molecules through modifications with different targeting groups.

By different surface passivation, C-dots may get corresponding groups on the surface, which can be conjugated or modified with other functional targeting molecules. For example, C-dots that were synthesized in water-glycol medium using glucose as carbon source could be modified with PEI to improve fluorescence quality. The as-prepared C-dots were then conjugated with CEA8 antibody to label and image HeLa cells *in vitro*. No apparent cytotoxicity was

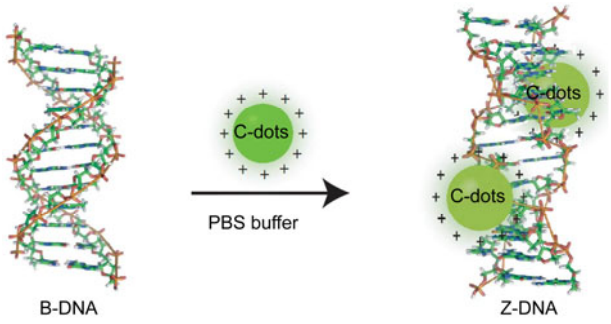

Figure 7 Schematic representation of the B-Z DNA transition induced by C-dots [29].

observed, demonstrating much better biosafety property compared with CdTe QDs [8]. More recently, Dong *et al.* [73] reported different C-dots that were synthesized by a solvothermal method with glucose as the carbon source and modified with 1,6-hexamethylene diamine. Such C-dots were then linked with mouse anti-human Alpha fetoprotein (AFP) antibody and goat anti-mouse IgG, respectively, to label human hepatocellular carcinoma cells, showing very strong fluorescence intensity for the effective detection of these cells. In addition, the fluorescent C-dots exhibited much better photostability and brighter fluorescence than FITC (fluoresceinisothiocyanate, a standard fluorescence marker), showing good application potential in the immunolabeling of cells. At the same time, none of the hepatocellular carcinoma cells showed any statistically significant group differences with respect to cell survival within 48 h. Moreover, C-dots have been applied in labeling microorganisms, such as germs. There have been evidences involving the use of C-dots as a powerful tool for labeling of *E.coli.* [31, 68, 74].

There were many reports focusing on the use of C-dots for fluorescence imaging *in vivo*. The oligomeric PEG-functionalized C-dots were evaluated *in vivo*, and the results suggested that these fluorescent dots were nontoxic to the selected cell lines (not more toxic than the oligomeric PEG molecules); neither did they impose any significant toxic effects on mice at dosages beyond those commonly used for *in vivo* optical imaging [62]. Both C-dots and ZnS-doped C-dots functionalized with PEG1500N were injected through three different routes (subcutaneously, intradermally, and intravenously) into female DBA/1 mice. Both types of C-dots could be excited through 470 nm and 545 nm filters. The ZnS-doped C-dots emitted stronger fluorescence than non-doped C-dots as shown in Figure 8. The PL from both types of injected dots faded in 24 h after injection. After intradermal injection into the front extremity, the C-dots migrated to the axillary lymph nodes, similar to CdSe/ZnS semiconductor QDs, but at a lower rate, presumably because PEG functionalization reduced their interaction with lymph cells. The fluorescence of axillary lymph

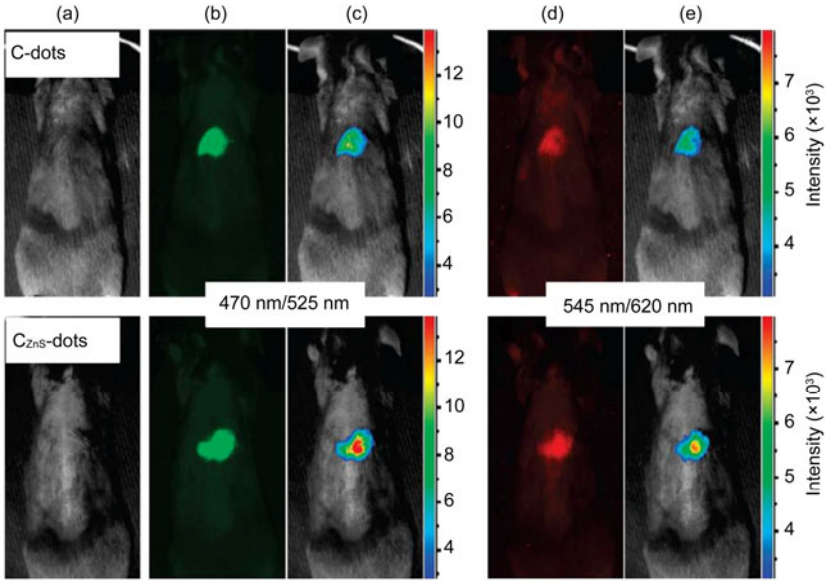

Figure 8 Subcutaneous injection of C-dots (top) and ZnS-C-Dots (bottom): (a) bright field, (b, d) as-detected fluorescence (excitation/emission wavelengths indicated), and (c, e) color-coded images [26].

nodes could readily be detected at 24 h post-injection. When injected intravenously for whole-body circulation studies, C-dots emission from the bladder area was observed, and PL could be detected in the urine, consistent with the expected renal excretion of the C-dots after 3 h injection. The results suggested that the intravenously injected C-dots were primarily excreted via urine, an excretion pathway that were widely reported in literature, especially for very small particles [75]. At 4 h after injection, organs were harvested and the C-dots were found to have accumulated in the kidneys (which was consistent with a urine excretion pathway) and scantly in the liver. Other organs including liver, spleen and kidneys showed very weak fluorescence at 4 h post-intravenous injection, suggesting a rather low accumulation level of the C-dots. Under the imaging conditions, the C-dots were photochemically stable, and did not show any significant signal degradation in repeated excitations for the continuous collection of fluorescence images [26]. Recently, Li *et al.* [76] reported that the blue fluorescent C-dots were detected in brain, suggesting that the C-dots might be able to cross the blood-brain barrier. Other experiments of the *in vivo* bioimaging by C-dots [25, 26, 31] also demonstrated that C-dots injected in various ways into mice remained strongly fluorescent *in vivo* and showed no noticeable signs of toxicity to the treated animals. Therefore, C-dots may offer great potential for optical imaging and related biomedical applications.

Longer wavelengths are usually preferred for *in vivo* optical imaging due to the improved photon tissue penetration and reduced background autofluorescence, especially in the NIR region. Recently, C-dots derived from MWNTs were chosen for *in vivo* fluorescence imaging [8]. A nude mouse was subcutaneously administered with C-dots at three different locations. Various excitations including blue, green, yellow, orange, red, deep red, and NIR light with center wavelengths at 455, 523, 595, 605, 635, 661, and 704 nm, respectively, were applied during *in vivo* imaging of the mouse. After spectral normalization to differentiate the background autofluorescence (green), the subcutaneously injected spots (red) on the mouse were seen in these fluorescence images under all different light excitations. Compared to images acquired using blue (455 nm) and green (523 nm) light excitation, those taken under longer wavelength excitations (595 nm and beyond) showed much better signal-to-background separation as shown in Figure 9. Although the fluorescence emission of C-dots was weaker at longer wavelengths, the tissue autofluorescence background decreased even more dramatically, resulting in an improved signal-to-noise ratio under red and NIR excitation. The capability of C-dots for NIR *in vivo* fluorescence imaging ($\lambda_{excitation}$ = 704 nm, $\lambda_{emission}$ = 770 nm) demonstrates the great potential of C-dots for use as optical nanoprobes in biomedical imaging (Figure 9) [8].

In comparison with down-conversion fluorescent materials, up-conversion materials have many advantages in biological applications, such as noninvasive and deep penetration of NIR radiation, the absence of autofluorescence of biological tissues, and feasibility of multiple labeling with different emissions under the same excitation [31, 64, 69, 77, 78]. C-dots could possess excellent up-conversion PL, due to the multiphoton active process. During this process, the simultaneous absorption of two or more photons led to the emission of light at a shorter wavelength than the excitation wavelength (anti-Stokes type emission). The C-dots prepared by one-step microwave pyrolysis of citric acid at low temperature in the presence of PEI exhibited good up-conversion

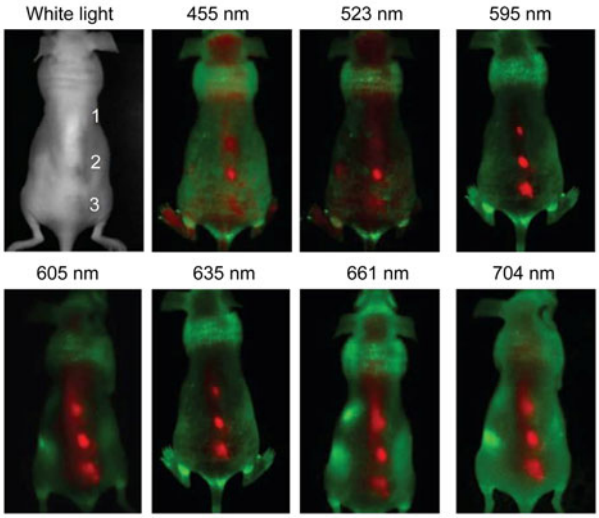

Figure 9 *In vivo* FL imaging of C-dots injected mouse. The images were taken under various excitation wavelengths at 455, 523, 595, 605, 635, 661 and 704 nm. Red and green represent the FL signals of C-dots and the tissue autofluorescence, respectively [8].

fluorescent properties besides their strong emission luminescence in the 450–650 nm range. Moreover, C-dots could be excited by long wavelength light (maximum intensity with 850 nm excitation) with the up-conversion emissions located in the range of 380–550 nm [79]. These C-dots have been successfully used for *in vitro* cell imaging with both one- and two-photon excitations [25, 31,80]. Sun *et al.* [80] reported that C-dots were strongly emissive in the visible region (458 nm) under either one-photon UV excitation or two-photon excitation in the near-infrared range (800 nm), indicating that the C-dots had two-photon active luminescence with excitation in the NIR range comparable to those of the best performing semiconductor QDs. Other groups also reported that C-dots prepared from different synthetic methods possessed obvious up-conversion PL properties [35, 49, 56, 78, 81, 82]. The C-dots passivated by propionylethylenimine-*co*-ethylenimine (PPEI-EI, with EI fraction 20%) were internalized in human cancer cells for two-photon luminescence microscopy imaging. As shown in Figure 10, the C-dots were strongly emissive with either 458 nm excitation or 800 nm two-photon excitation. Inside the cells, C-dots accumulated preferentially in the membrane and the cytoplasm. The one- and two-photon luminescence images for the same scanning area matched quite well. The C-dots were photostable under the two-photon imaging conditions (upon repeated 800 nm excitations equivalent to generating the image for at least 3000 times, no significant changes in emission intensities were observed). The performance of C-dots as two-photon imaging sensors was found to be comparable to that of the best performing semiconductor QDs [80].

For bioimaging applications, further research is required to establish the protocols for C-dots synthesis and functionalization to target specific cell types and/or specific cell

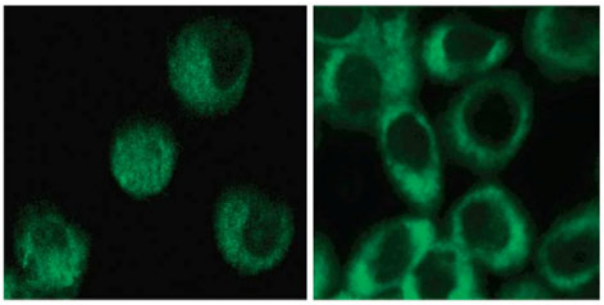

Figure 10 Representative two-photon luminescence image (800 nm excitation) of human breast cancer MCF-7 cells with internalized C-dots [80].

compartments. Through suitable doping, chemical manipulation, or incorporation into nanocomposites, C-dots may open a door to a host of unforeseen applications, such as contrast agents for magnetic resonance imaging (MRI) [3]. The evaluation of C-dots *in vivo* is still at its beginning stage, but with bright prospects. The synthesis of C-dots with bright fluorescence in the red/near-IR spectral regions and/or multiphoton-based emissions can be explored for further development.

3.2 Biosensor

C-dots can serve as either excellent electron donors or electron acceptors, and their PL can be accordingly quenched efficiently by either electron acceptor or electron donor molecules in solution [30]. Based on their excellent properties and biocompatibility, C-dots can be designed for biosensors to detect metal ions, biological pH, sugars, proteins, enzymes, nucleic acid, etc.

C-dots based ratiometric fluorescent assays were reported to give high specificity and sensitivity for *in vivo* imaging and sensing of metal ions. By integration with *N*-(2-aminoethyl)-*N*,*N*,*N*′-tris(pyridin-2-ylmethyl)ethane-1, 2-diamine (AE-TPEA), the C-dots can be used for Cu^{2+} ion sensing because AE-TPEA can recognize Cu^{2+} ion with high specificity and long-term stability [83]. In another report, C-dots were employed to detect Cu^{2+} ion using both down and up-conversion fluorescence. The C-dots was prepared by microwave pyrolysis of citric acid at low temperature in the presence of PEI. The resultant C-dots exhibited good up-conversion fluorescent properties besides their strong emission luminescence in the 450–650 nm range, and could be excited by long wavelength light (maximum intensity with 850 nm excitation) with the up-conversion emissions located in the range of 380–550 nm [79]. Both fluorescent nanosensors showed low cytotoxicity and good cell permeability, thus they could be successfully applied for intracellular sensing of Cu^{2+} in biological systems. Detection of other ions was also achieved by conjugating the C-dots with corresponding ligands.

Besides the metal ions, the physiological pH in living

cells and tissues can be detected by C-dots. C-dots functionalized with –COOH and/or –OH groups were synthesized by electrochemical method and then integrated with aminomethylphenylterpyridine (AE-TPY). In this case, the C-dots could be used as receptors, responsive to the concentration change of H^+. The integrated C-dots-TPY exhibited fluorescent emission in the visible region by two-photon excitation at the wavelength of 800 nm. This two-photon fluorescent probe was suitable for monitoring pH gradients in a range of 6.0–8.5 with high sensitivity and selectivity, and was successfully employed in living cells (human lung cancer A549 cells and mouse LLC-MK2 cells) and tumor tissues of nude mice at depth of 65–185 μm without interference with other biologically relevant species [84].

A C-dots based strategy for DNA sensing was proposed by Li *et al.* [85]. C-dots with the size of tens of nanometers from candle soot could be used as an immobilization support for a labeled single-stranded DNA (ssDNA), resulting in the quenching of the probe. Upon hybridization with the target DNA to form double-stranded DNA (dsDNA), desorption from C-dots occurred, thus the recovery of fluorescence could be measured quantitatively. Relatively higher dimension C-dots were required for this application because smaller C-dots were highly fluorescent and could interfere with detection of the probe signal. Wang *et al.* [86] developed another protocol to detect DNA based on the CL of C-dots triggered by potassium permanganate. Under optimal conditions, this paper-based DNA sensor performed quite well, with a linear range of 10^{-18} to 10^{-14} M and with a detection limit of 8.56×10^{-19} M for target DNA. They concluded that this DNA sensor, providing high-throughput, rapid, sensitive, stable and reusable CL response, might be very useful for the detection of trace amounts of analyte in real biological samples.

Subhabrata *et al.* [87] prepared C-dots-dsDNA hybrid simply through electrostatic attraction for histone detection. The emission of C-dots could be quenched in presence of dsDNA. Interestingly, addition of histone into this C-dots-dsDNA hybrid turned on the fluorescence signal of C-dots through unwinding dsDNA from C-dots surface due to the strong binding affinity between histone and dsDNA. Consequently, the unbound (free) C-dots exhibited its native fluorescence. Thus, simply by monitoring the fluorescence quenching (off) and restoration (on), a label-free histone sensing technique was developed with a detection limit of 0.2 ng/mL, which was two orders of magnitude more sensitive than previously reported methods.

An aptamer-based turn-on thrombin biosensor was constructed by using aptamer-bridged phosphorescent energy transfer, with the Mn-doped ZnS QDs labeled with thrombin-binding aptamer as donors, and C-dots as acceptors. Due to the π-π stacking interaction between aptamer and C-dots, the energy donor and acceptor were taken into close proximity, leading to the phosphorescence quenching of the donor. A maximum phosphorescence quenching efficiency could reach as high as 95.9%. With the introduction of thrombin to the "off state" of this donor-acceptor system, the phosphorescence was "turned on" upon the formation of quadruplex-thrombin complexes. Based on the restored phosphorescence, the sensor displayed a linear detection range of 0–40 nM for thrombin, with detection limit of as low as 0.013 nM in pure buffers. The proposed sensor can be used to monitor thrombin in complex biological fluids, including serum and plasma, with satisfactory recovery [88].

C-dots based fluorescence resonance energy transfer (FRET) sensing is an emerging means in C-dots employed biosensors. FRET system is a widely adopted ratiometric sensing protocol because the detection index using the ratio of two interconnected fluorescence signals can effectively eliminate the influence of variations caused by factors such as temperature and local probe concentration. Yu *et al.* [89] developed a C-dots based FRET ratiometric fluorescent sensor for detecting H_2S in aqueous media and serum, as well as inside living cells. C-dots were anchored with naphthalimide-azide derivative and served as the energy donor. This C-dots-naphthalimide-azide sensor demonstrated a detection limit of 10 nM, the lowest among fluorescent H_2S sensors. Moreover, this sensor showed a large shift (190 nm) between donor excitation and acceptor emission, which could exclude any influence of excitation backscattering effects on fluorescence detection. In addition to its selective detection of H_2S in aqueous media and in serum samples, the sensor can also permeate the cell membrane and realize H_2S imaging in living cells. Taking advantage of FRET, Yu's group [90] also designed a C-dots based nanosensor which is highly selective for NO both in water and in living cells. In this system, C-dots not only served as an energy donor, but also provided the anchoring site for phenylenediamine-containing naphthalimide, the NO probe moiety. Such C-dots would become an energy acceptor in the presence of NO, causing the fluorescence change from blue to green. More recently, a multifunctional fluorescent nanoprobe was applied in the detection of mitochondrial H_2O_2 by conjugating a mitochondria-targeting ligand and a H_2O_2 recognition element onto C-dots [91]. Exogenous H_2O_2 in L929 cells and endogenously produced mitochondrial H_2O_2 in RAW 264.7 cells were successfully detected and the limit of detection was determined as 0.75 μM. This research pushed the C-dots based FRET detection forward to the subcellular level.

CL was defined as the production of light through a chemical reaction. C-dots have been considered to be a promising CL reagent compared with other CL reagents. CL properties of C-dots were observed in the presence of potassium permanganate ($KMnO_4$), cerium (IV) (ammonium ceric sulfate), hydrogen peroxide or peroxynitrous acid [39, 86, 92, 93]. Recently, the CL behavior of C-dots was also detected in the presence of a strong alkaline solution, such as NaOH or KOH, with the CL intensities dependent on the

concentration of the base [94]. Shi *et al.* [95] established a biosensor for Co (II) based on the CL of C-dots excited by ·OH radicals, which were produced by Co (II) triggered Fenton-like reaction. Under optimized experimental conditions, this CL system exhibited a reliable response to Co (II) from 1.0 to 1000 nM with a detection limit of 0.67 nM. Moreover, this system was successfully used for the detection of Co (II) in HepG2 cells, and the experimental results agreed with those obtained by inductively coupled plasma mass spectrometry (ICP-MS) method.

As ECL is extensively used to investigate the fluorescent emission of QDs or semiconductor nanocrystals, ECL studies of C-dots have attracted great interest. The ECL behavior of C-dots was similar to that of QDs such as CdSe and Si nanocrystals. More importantly, ECL response was relatively stable over time, which implied attractive applications in ECL sensing [96]. Recently, an ECL platform for ultrasensitive and selective detection of leukemia cells was reported. In the platform, the mesoporous gold with controllable three-dimensional porosity and good conductivity was used to modify the screen-printed carbon electrode. C-dots coated ZnO nanospheres (ZnO@C-dots) were used as good ECL labels with low cytotoxicity and good biocompatibility. The aptamer was used for cell capture and the concanavalin A conjugated ZnO@C-dots was used for selective recognition of the cell surface carbohydrate. The proposed method showed a good analytical performance for the detection of K562 cells ranging from 1.0×10^2 to 2.0×10^7 cells/mL with a detection limit of 46 cells/mL [97].

The biosensor based on C-dots has the advantages of high sensitivity, good cell-permeability, low cytotoxicity, strong specificity, and good stability, providing great promise for efficient bio-related detection.

3.3 Disease-detection system

The importance of fluorescent nanoprobes in biomedical research and practice has been rapidly increasing as a converged outcome of recent developments in fluorescence microscopy, laser technologies, and nanotechnology. Benign "nanolanterns" has always been a hot topic due to their potential for studying intracellular transport and biochemical interactions, which can ultimately be used for disease detection and therapy [98].

Qin *et al.* [99] designed a glucose biosensor based on electrochemical method. The glucose oxidase (GOD) self-assembled into the C-dots-reduced graphene oxide (C-dots-rGO) hybrids. Then the glucose biosensor was constructed by deposition of the GOD-C-dots-rGO hybrids on the surface of a glassy carbon electrode. The glucose was detected by the electrochemical method, with a linear detection range from 40 μM to 20 mM (r = 0.994). This glucose biosensor can be used to detect glucose in human blood serum, the abnormity of which might be an indicator of a variety of diseases such as diabetes and cirrhosis.

Li *et al*. [98] passivated C-dots with linear PEG, 4-armed PEG and PEI-PEG-PEI, respectively. After conjugation with transferrin, these C-dots could target cancer cells and were used as biocompatible optical nanoprobes for *in vitro* cancer diagnostics (Figure 11). In a separate study by Song *et al.* [100], folic acid (FA) was conjugated to the surface of C-dots by amidation, providing an efficient approach to discriminate cancer cells from normal cells via receptor-mediated endocytosis.

Recently, polyamidoamine dendrimers capped-C-dots (PAMAM-C-dots) were fabricated by one-step microwave assisted pyrolysis of citric acid and PAMAM. The obtained graphitic PAMAM-C-dots, with abundant amine groups, were employed as reducing and capping agents in the formation of PAMAM-C-dots/Au nanocrystal nanocomposite. The resulting nanocomposite exhibited excellent conductivity, stability and biocompatibility on the surface of electrode, and was designed as an immobilized matrix for sensitive immune sensing of alpha-feto protein (AFP), showing a wide linear detection range from 100 fg/mL to 100 ng/mL. The detection limit for AFP was 0.025 pg/mL. Importantly, the immune sensor was evaluated for the analysis of clinical

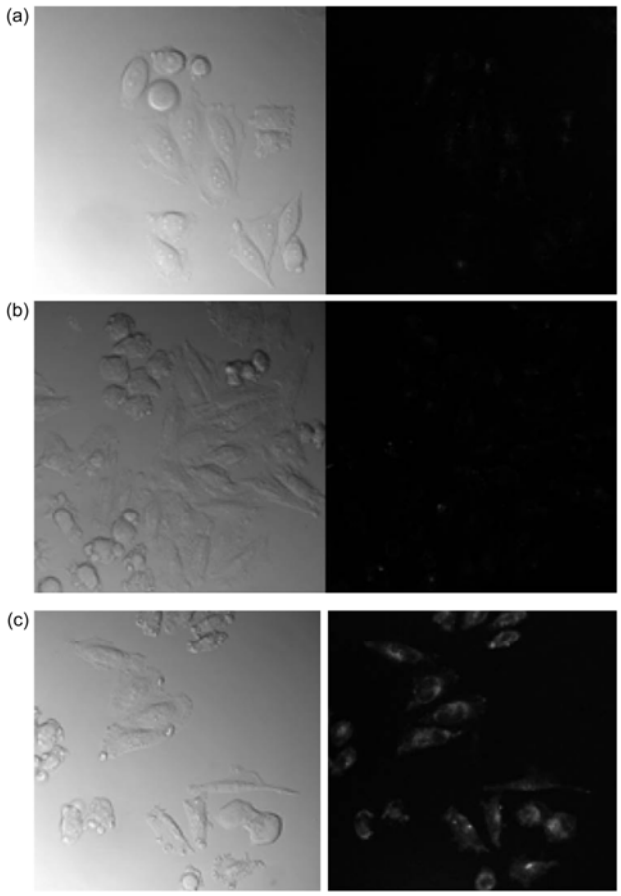

Figure 11 Targeting HeLa cells with transferrin conjugated carbon dots. (a) HeLa cells incubated with C-dots; (b) the cells incubated with transferrin-coupled C-dots; and (c) the cells incubated with transferrin-coupled C-dots after transferrin pretreatment [98].

serum samples, giving a good correlation with enzyme-linked immune sorbent assay (ELISA). The results indicated that the immune sensor provided a possible protocol for the detection of AFP in clinical diagnosis [101].

A sensitive ECL immunosensor for the detection of prostate protein antigen (PSA) was developed by Wu *et al.* The graphene conjugated with gold nanoparticles (AuNPs) (GR@AuNPs) was used to modify glassy carbon electrode (GCE), providing an effective matrix for anti-AFP immobilization. C-dots simply prepared by electro oxidation of graphite was used as ECL reagent and loaded into the nanoporous sliver (NPS), forming the NPS@C-dots composites as good ECL labels. The good electrical conductivity of GR@AuNPs and NPS@C-dots composites provided significant advantage of dual-signal amplification technique. By characterizing the ECL intensity with different concentration of PSA, this biosensor displayed good analytical performance for the detection of PSA in the range from 1 pg/mL to 50 ng/mL with a low detection limit of 0.5 pg/mL. Moreover, the sensor showed good reproducibility, acceptable precision and reliable stability, thus could provide many potential applications in the detection of tumor maker in clinical research [102].

A fluorescence imaging guided photodynamic therapy (PDT) system, which was based on the chlorin e6 (Ce6, a photosensitizer) conjugated C-dots (C-dots-Ce6), was reported by Huang *et al.* C-dots, as the carrier to load photosensitizers (PSs) or dyes, have the following advantages: (i) C-dots can improve the stability, solubility, biocompatibility, circulation half-life and tumor-homing ability of PSs or dyes in aqueous/biological media; (ii) C-dots can permeate barriers including cell membranes and fenestrated vasculature in the cancer area and increase the ingestion of tumor tissue; (iii) C-dots can indirectly excite the PSs or dyes by FRET mechanism. C-dots-Ce6 was injected into the left rear flank area of mice for *in vivo* fluorescence imaging, and the subcutaneous injection site displayed a strong fluorescence signal. The area of the fluorescence signal gradually expanded from center, suggesting that C-dots-Ce6 had good distribution ability in tissue. This can be attributed to its good stability and dispersibility in aqueous systems. Later on, nude mice with subcutaneous MGC803 gastric cancer xenograft were selected as the animal model to evaluate the *in vivo* fluorescence imaging-guided PDT (Figure 12). NIR fluorescence imaging was employed to monitor PDT *in vivo* after the mice were treated with intravenous injection of C-dots-Ce6. Significant fluorescence emitted from the C-dots-Ce6 injected mice was observed in the tumor area. Meanwhile, there was also fluorescence signal in the other tissues. The average fluorescence intensity from Ce6 acquired in the tumor areas quickly arose within 24 h post-injection and reached a plateau in 48 h post-injection, followed by steady decrease over time. According to the observation from NIR fluorescence imaging, 8 h post-injection

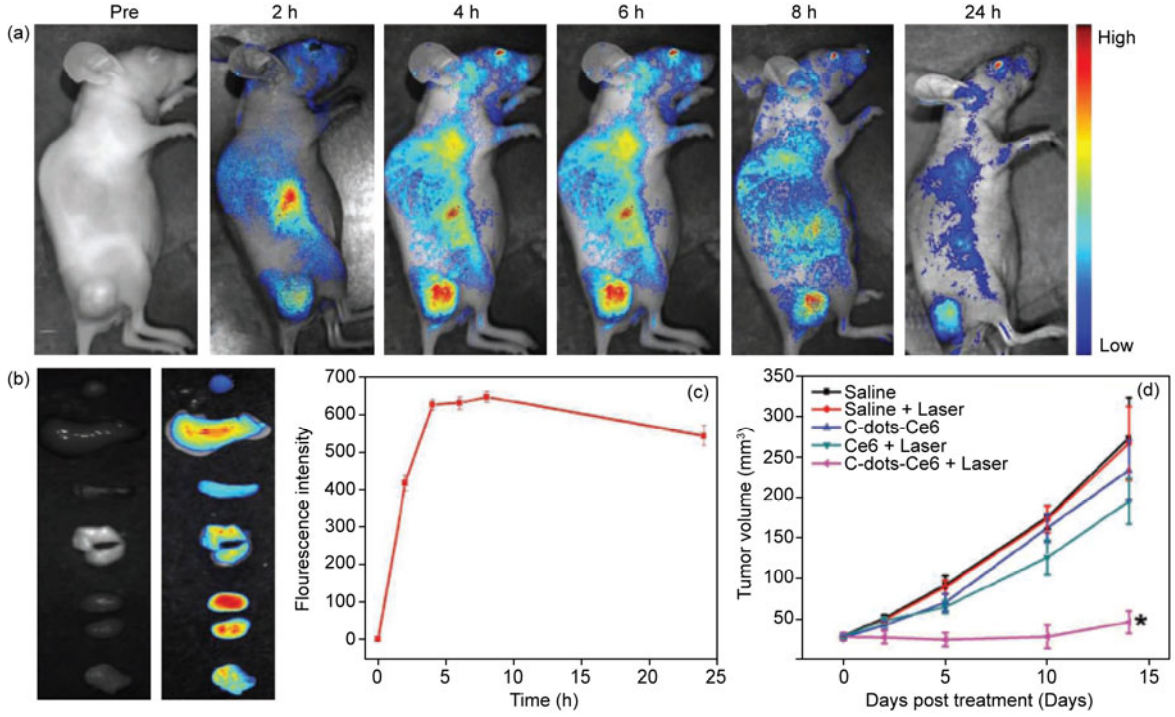

Figure 12 (a) Real-time *in vivo* NIR fluorescence images after intravenous injection of C-dots-Ce6 in nude mice at different time points; (b) ex vivo images of mice tissues (from top to bottom: heart, liver, spleen, lung, kidneys, tumor); (c) the average fluorescence intensities from the tumor area at 24 h post-injection (n = 5); (d) MGC803 tumor growth curves after various treatments (n = 5). (∗, $p < 0.05$ for other groups versus C-dots-Ce6 + laser group) [103].

was selected as the suitable time point to implement PDT. The tumor area was irradiated for 10 min using a 671 nm laser (Figure 12). The C-dots-Ce6 administration/irradiation group showed partial tumor regression. These results indicated that C-dots-Ce6 had excellent imaging and tumor-homing ability without compromising the photodynamic efficacy, and was suitable for simultaneous PFD and PDT of tumor *in vivo*. Great potential is expected for applications in the clinic to treat patients with gastric cancer or other tumors [103].

For bioanalytical applications, research is focused on increasing the sensitivity and the selectivity of the nanosensors and on lifetime-based detection methodologies. Taking this into consideration, C-dots are particularly suitable for biological sample analysis [104].

3.4 Gene and drug delivery system

Over the past few decades, gene therapy, involving delivery of appropriate exogenous genes (DNA or RNA) into cells and their expression for specific enhancing or suppressing effects, has been regarded as a promising cure for life-threatening diseases. A variety of drug delivery systems, such as lipid- or polymer-based nanoparticles, have been designed to improve the pharmacological and therapeutic properties of drugs. Imaging plays indispensable roles in tracing, diagnosis, treatment, and confirmation of therapy, hence promoting the development of "theranostics" for simultaneous disease diagnosis and therapy, in both gene and drug delivery systems. Due to their excellent fluorescence performance, small sizes, low cytotoxicity and good transmembrane ability, C-dots are becoming a competent candidate for imaging-concomitant gene and drug delivery.

Zhou *et al.* [105] designed a nanocomposite system to respond to physiopathological pH signals to trigger drug release in cancerous cells and serve as imaging agents in the transport process to their destination. First, the carboxylic groups functionalized C-dots (3.8 nm) were prepared by a one-step pyrolytic route from ethylenediamine-tetra acetic acid salts. The C-dots equipped with many carboxylic acid moieties at the surface imparted them with excellent water solubility. The anticancer drug doxorubicin (DOX) was loaded into the pores of the aminopropyl group functionalized mesoporous silica nanoparticles (MSPs, with an average pore diameter of 2.5 nm, and a narrow pore distribution), then the negatively charged C-dots were anchored to MSPs through electrostatic interaction and were utilized as caps for trapping the guest molecules within the pores. It was found that adjusting the system to mildly acidic condition at physiological temperature caused the dissociation of the C-dots@MSPs complex, releasing a large quantity of DOX from the nanospheres. The endocytosis and the efficient drug release properties of the system were further confirmed by luminescence microscopy. Moreover, the DOX-loaded nanocomposites exhibited a remarkably enhanced efficiency in killing cancer cells. Owing to its excellent optical property, C-dots@MSPs were used for *in vivo* optical imaging by subcutaneous injection into the nude mice and applied for PL imaging. As expected, the corresponding injection site of the mouse displayed a clear PL signal, suggesting that C-dots@MSPs might offer great potential for tracking the *in vivo* delivery of therapeutic agents. In another drug delivery study by Lai *et al.* [33], C-dots with PEG functionalization were applied. The DOX loaded on the dots exhibited higher toxicity to HeLa cells than free DOX, and the fluorescence imaging results suggested that the release of DOX from the carrier C-dots likely occurred inside the cells. Chen *et al.* [106] found that calcination at 400 °C could grant mesoporous organosilica nanoparticles with strong fluorescence, which was originated from the C-dots formed in the calcination. DOX can be efficiently encapsulated into these fluorescent mesoporous silica nanoparticles. After coupled to c(RGDyK), the nanoconjugates could be efficiently localized to tumors through interactions with integrin $\alpha_v\beta_3$ overexpressed on the tumor vasculature.

Recently, very interesting hollow C-dots were prepared from bovine serum albumin (BSA) by solvothermal reaction for drug delivery. The process of the formation of hollow C-dots was described briefly. First, BSA monomers dispersed in solution tend to form aggregates of uniform size after ultrasonication. After solvothermal treatment for 8 h, BSA was denatured, and carbonization could be found on the surface of small aggregates of denatured BSA. The incompletely carbonized interior of the nanoparticles may prevent the shell from sinking or breaking. Finally, after solvothermal treatment for 8 h, the incompletely carbonized interior was carbonized, producing hollow C-dots (Figure 13). The obtained hollow C-dots showed 6.8 nm in diameter and a hollow structure with a pore size of ca. 2 nm and had a QY of 7% and bright PL. Luminescent hollow C-dots were prepared as a delivery vehicle for DOX, exhibiting pH-controlled release and rapid absorption by cells. Because of their specific nanostructure and photoluminescent properties, the multifunctional hollow C-dots show potential for application in both cell imaging and cancer therapy [107].

In our previous study, PEI25k-passivated C-dots prepared by one step microwave assisted pyrolysis of glycerol in the presence of branched PEI25k were found to have positive charges on the surface, thus being polyelectrolyte-like to condense DNA (Figure 14). The gene expression of plasmid DNA delivered by the C-dots was competitive to that by PEI25k in COS-7 cells and HepG2 cells. In addition to the delivery, the C-dots were also used for optical imaging. The COS-7 cells were stained by C-dots after 3 h incubation, and the stained cells exhibited blue, green, and red fluorescence emissions with 405, 488, and 543 nm excitations, respectively (Figure 14). Inside the cells, the C-dots were mostly trapped in endosomal compartments, without significant penetration into the cell nucleus [21]. More recently, C-dots were used as a visible tool to monitor

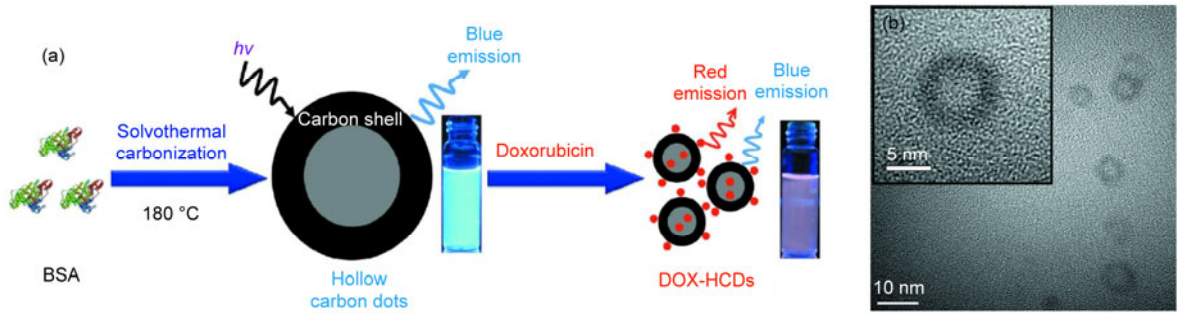

Figure 13 (a) Graphical illustration of the synthesis of hollow C-dots and the loading and delivery of DOX; (b) HRTEM image and magnification (inset) of the hollow structure of hollow C-dots [107].

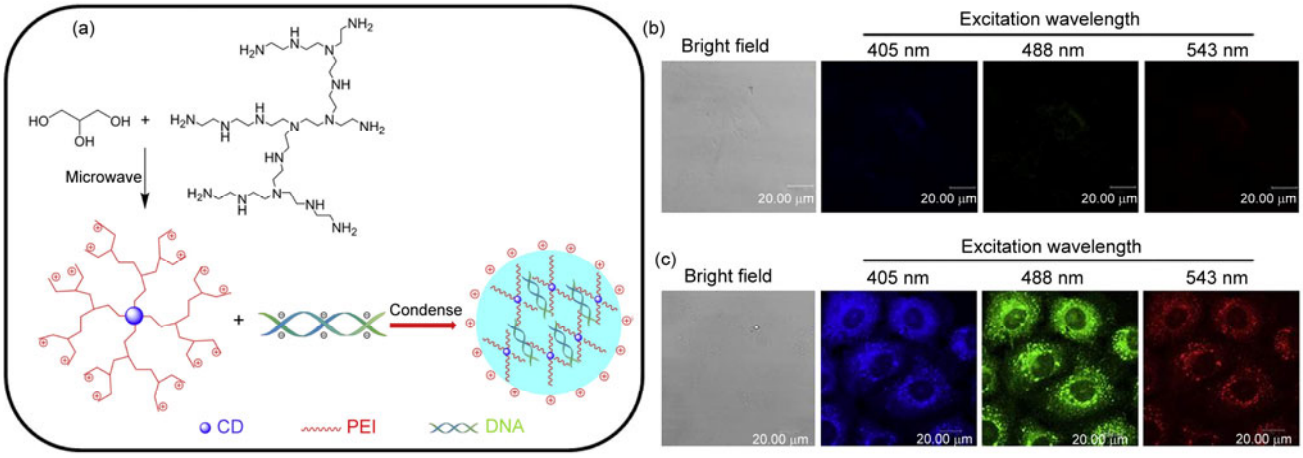

Figure 14 (a) Depiction of the formation of C-dots surface passivated with PEI25k (PEI-C-dots) and PEI-C-dots/pDNA complex and laser scanning confocal microscopy images of non-transfected cells as negative controls (b) and transfected cells (c). The samples were observed under bright field and excited at 405, 488 and 543 nm [21].

the association/dissociation of polymeric carrier/plasmid DNA (pDNA) complex during transfection in a non-labeled manner, providing an efficient strategy to study the mechanism of polymer-mediated pDNA delivery. The surfaces of C-dots and Au were modified with PEI and subsequently treated with non-labeled pDNA to form the C-dots-PEI/pDNA/Au-PEI complex via electrostatic interaction (Figure 15). Au nanoparticles were employed to quench the fluorescence of C-dots when they became close with each other. The dissociation of the complex in cells caused accompanied fluorescence recovery due to the increase in distance between C-dots and Au (Figure 15). Compared to PEI25k, C-dots-PEI/Au-PEI carrier showed high efficiency and low cytotoxicity. At the same time, the changes that occurred at the intracellular level during transfection especially post-endosomal steps were monitored by fluorescence measurement using fluorescence microscope [108].

More evaluations on C-dots based platforms for potential applications in gene and drug delivery (simultaneous delivery and imaging), especially single-particle platform to track living cells are worthy of great attentions.

4 Summary and outlook

Since the discovery of C-dots ten years ago, researches on the synthesis, performance, mechanism and application of C-dots have sprung up rapidly. Various kinds of convenient scalable synthesis methods, the properties of emission-color tuning and a non-blinking behavior coupled with a high photo and chemical stability *in vitro* and *in vivo*, negligible toxicity for cells or living bodies, higher and higher QYs have attracted tremendous attentions of researchers and resulted in extensive applications. In biological applications, C-dots have significant potential to serve as nontoxic replacements to traditional heavy-metal based QDs. Additionally, the facile introduction of versatile functionality at the C-dots surface without influencing FL properties enriched their applications, especially in the targeted delivery or therapy.

As new comers to nanomaterial family, C-dots are undoubtedly showing great potential in a wide variety of applications in their own right; however accurate control over their properties is still far from ideal. For example, due to the small size of C-dots prepared from most synthetic

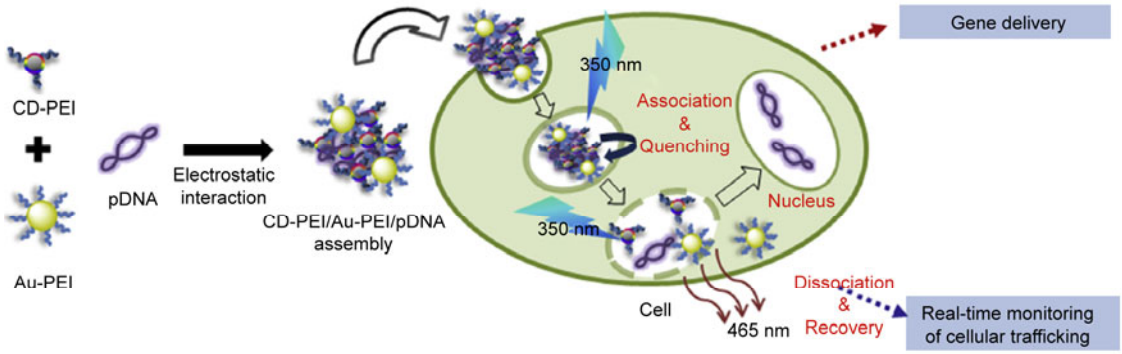

Figure 15 A schematic illustration for the gene delivery and real-time monitoring of cellular trafficking utilizing C-dots-PEI/Au-PEI/pDNA molecular assembly of nanohybrids [108].

methods and their low density nature, it is uneasy to effectively purify them simply by centrifugation, sedimentation or dialysis. In fact, many nanodots lack uniformity in sphericity and usually show dispersity in size. Most preparation processes involve complicated chemical reactions such as pyrolysis and carbonization, leading to intricate structures that are inconvenient in characterization with NMR, IR, etc. Meanwhile, the origins of their PL remain controversial and better clarification is still required. More detailed fundamental studies on the properties of C-dots are of great urgency now. The mechanism of photophysical properties of C-dots is worthy of further research and discussion. And for further development, more attention is needed for the synthesis of C-dots with bright fluorescence in the red/near-IR spectral regions and/or multiphoton-based emissions. It is hopeful that various kinds of nanodevices based on C-dots will be applied in biological field in clinic.

The authors gratefully acknowledge the support for this work from the National Science and Technology Major Project of China (2012ZX-10004801-003-007, 2012AA022603).

1 Xu XY, Ray R, Gu YL, Ploehn HJ, Gearheart L, Raker K, Scrivens WA. Electrophoretic analysis and purification of fluorescent single-walled carbon nanotube fragments. *J Am Chem Soc*, 2004, 126: 12736–12737
2 Li HT, Kang ZH, Liu Y, Lee ST. Carbon nanodots: synthesis, properties and applications. *J Mater Chem*, 2012, 22: 24230–24253
3 Baker SN, Baker GA. Luminescent carbon nanodots: emergent nanolights. *Angew Chem Int Ed*, 2010, 49: 6726–6744
4 Esteves da Silva JCG, Goncalves HMR. Analytical and bioanalytical applications of carbon dots. *Trac-Trend Anal Chem*, 2011, 30: 1327–1336
5 Luo PJG, Sahu S, Yang ST, Sonkar SK, Wang JP, Wang HF, LeCroy GE, Cao L, Sun YP. Carbon "quantum" dots for optical bioimaging. *J Mater Chem B*, 2013, 1: 2116–2127
6 Li XY, Wang HQ, Shimizu Y, Pyatenko A, Kawaguchi K, Koshizaki N. Preparation of carbon quantum dots with tunable photoluminescence by rapid laser passivation in ordinary organic solvents. *Chem Commun*, 2011, 47: 932–934
7 Qiao ZA, Wang YF, Gao Y, Li HW, Dai TY, Liu YL, Huo QS. Commercially activated carbon as the source for producing multicolor photoluminescent carbon dots by chemical oxidation. *Chem Commun*, 2010, 46: 8812–8814
8 Tao HQ, Yang K, Ma Z, Wan JM, Zhang YJ, Kang ZH, Liu Z. *In vivo* NIR fluorescence imaging, biodistribution, and toxicology of photoluminescent carbon dots produced from carbon nanotubes and graphite. *Small*, 2012, 8: 281–290
9 Ding H, Cheng LW, Ma YY, Kong JL, Xiong HM. Luminescent carbon quantum dots and their application in cell imaging. *New J Chem*, 2013, 37: 2515–2520
10 Wu ZL, Zhang P, Gao MX, Liu CF, Wang W, Leng F, Huang CZ. One-pot hydrothermal synthesis of highly luminescent nitrogen-doped amphoteric carbon dots for bioimaging from bombyx mori silk-natural proteins. *J Mater Chem B*, 2013, 1: 2868–2873
11 Puvvada N, Kumar BNP, Konar S, Kalita H, Mandal M, Pathak A. Synthesis of biocompatible multicolor luminescent carbon dots for bioimaging applications. *Sci Technol Adv Mat*, 2012, 13: 045008
12 Yang ZC, Wang M, Yong AM, Wong SY, Zhang XH, Tan H, Chang AY, Li X, Wang J. Intrinsically fluorescent carbon dots with tunable emission derived from hydrothermal treatment of glucose in the presence of monopotassium phosphate. *Chem Commun*, 2011, 47: 11615–11617
13 Wang F, Pang SP, Wang L, Li Q, Kreiter M, Liu CY. One-step synthesis of highly luminescent carbon dots in noncoordinating solvents. *Chem Mater*, 2010, 22: 4528–4530
14 Sahu S, Behera B, Maiti TK, Mohapatra S. Simple one-step synthesis of highly luminescent carbon dots from orange juice: application as excellent bio-imaging agents. *Chem Commun*, 2012, 48: 8835–8837
15 Wang QL, Zheng HZ, Long YJ, Zhang LY, Gao M, Bai WJ. Microwave-hydrothermal synthesis of fluorescent carbon dots from graphite oxide. *Carbon*, 2011, 49: 3134–3140
16 Peng H, Travas-Sejdic J. Simple aqueous solution route to luminescent carbogenic dots from carbohydrates. *Chem Mater*, 2009, 21: 5563–5565
17 Chowdhury D, Gogoi N, Majumdar G. Fluorescent carbon dots obtained from chitosan gel. *RSC Adv*, 2012, 2: 12156–12159
18 Zhang P, Li WC, Zhai XY, Liu CJ, Dai LM, Liu WG. A facile and versatile approach to biocompatible "fluorescent polymers" from polymerizable carbon nanodots. *Chem Commun*, 2012, 48: 10431–10433
19 Mitra S, Chandra S, Kundu T, Banerjee R, Pramanik P, Goswami A. Rapid microwave synthesis of fluorescent hydrophobic carbon dots. *RSC Adv*, 2012, 2: 12129–12131
20 Zhai XY, Zhang P, Liu CJ, Bai T, Li WC, Dai LM, Liu WG. Highly luminescent carbon nanodots by microwave-assisted pyrolysis. *Chem Commun*, 2012, 48: 7955–7957
21 Liu CJ, Zhang P, Zhai X, Tian F, Li W, Yang J, Liu Y, Wang H,

Wang W, Liu W. Nano-carrier for gene delivery and bioimaging based on carbon dots with pei-passivation enhanced fluorescence. *Biomaterials*, 2012, 33: 3604–3613
22 Liu CJ, Zhang P, Tian F, Li WC, Li F, Liu WG. One-step synthesis of surface passivated carbon nanodots by microwave assisted pyrolysis for enhanced multicolor photoluminescence and bioimaging. *J Mater Chem*, 2011, 21: 13163–13167
23 Wang W, Li YM, Cheng L, Cao ZQ, Liu WG. Water-soluble and phosphorus-containing carbon dots with strong green fluorescence for cell labeling. *J Mater Chem B*, 2014, 2: 46–48
24 Tan MQ, Zhang LX, Tang R, Song XJ, Li MY, Wu H, Wang YF, Lv GJ, Liu WF, Ma XJ.. Enhanced photo luminescence and characterization of multicolor carbon dots using plant soot as a carbon source. *Talanta*, 2013, 115: 950–956
25 Sun YP, Wang X, Lu FS, Cao L, Meziani MJ, Luo PJG, Gu LR, Veca LM. Doped carbon nanoparticles as a new platform for highly photoluminescent dots. *J Phys Chem C*, 2008, 112: 18295–18298
26 Yang ST, Cao L, Luo PGJ, Lu FS, Wang X, Wang HF, Meziani MJ, Liu YF, Qi G, Sun YP. Carbon dots for optical imaging *in vivo*. *J Am Chem Soc*, 2009, 131: 11308–11309
27 Ray SC, Saha A, Jana NR, Sarkar R. Fluorescent carbon nanoparticles: synthesis, characterization, and bioimaging application. *J Phys Chem C*, 2009, 113: 18546–18551
28 Zhang JC, Shen WQ, Pan DY, Zhang ZW, Fang YG, Wu MH. Controlled synthesis of green and blue luminescent carbon nanoparticles with high yields by the carbonization of sucrose. *New J Chem*, 2010, 34: 591–593
29 Feng LY, Zhao AD, Ren JS, Qu XG. Lighting up left-handed z-DNA: photoluminescent carbon dots induce DNA B to Z transition and perform DNA logic operations. *Nucl Acids Res*, 2013, 41: 7987–7996
30 Wang X, Cao L, Lu FS, Meziani MJ, Li H, Qi G, Zhou B, Harruff BA, Kermarrec F, Sun YP. Photoinduced electron transfers with carbon dots. *Chem Commun*, 2009: 3774–3776
31 Sun YP, Zhou B, Lin Y, Wang W, Fernando KAS, Pathak P, Meziani MJ, Harruff BA, Wang X, Wang HF, Luo PJG, Yang H, Kose ME, Chen BL, Veca LM, Xie SY. Quantum-sized carbon dots for bright and colorful photoluminescence. *J Am Chem Soc*, 2006, 128: 7756–7757
32 Liu HP, Ye T, Mao CD. Fluorescent carbon nanoparticles derived from candle soot. *Angew Chem Int Edit*, 2007, 46: 6473–6475
33 Lai CW, Hsiao YH, Peng YK, Chou PT. Facile synthesis of highly emissive carbon dots from pyrolysis of glycerol; gram scale production of carbon dots/mSiO_2 for cell imaging and drug release. *J Mater Chem*, 2012, 22: 14403–14409
34 Eda G, Lin YY, Mattevi C, Yamaguchi H, Chen HA, Chen IS, Chen CW, Chhowalla M. Blue photoluminescence from chemically derived graphene oxide. *Adv Mater*, 2010, 22: 505–509
35 Li HT, He XD, Kang ZH, Huang H, Liu Y, Liu JL, Lian SY, Tsang CHA, Yang XB, Lee ST. Water-soluble fluorescent carbon quantum dots and photocatalyst design. *Angew Chem Int Ed*, 2010, 49: 4430–4434
36 Wei WL, Xu C, Ren JS, Xu BL, Qu XG. Sensing metal ions with ion selectivity of a crown ether and fluorescence resonance energy transfer between carbon dots and graphene. *Chem Commun*, 2012, 48: 1284–1286
37 Goncalves H, Esteves da Silva JCG. Fluorescent carbon dots capped with PEG(200) and mercaptosuccinic acid. *J Fluoresc*, 2010, 20: 1023–1028
38 Chen PC, Chen YN, Hsu PC, Shih CC, Chang HT. Photoluminescent organosilane-functionalized carbon dots as temperature probes. *Chem Commun*, 2013, 49: 1639–1641
39 Lin Z, Xue W, Chen H, Lin JM. Peroxynitrous-acid-induced chemiluminescence of fluorescent carbon dots for nitrite sensing. *Anal Chem*, 2011, 83: 8245–8251
40 Huang QT, Hu SR, Zhang HQ, Chen JH, He YS, Li FM,Weng W, Ni JC, Bao XX, Lin Y. Carbon dots and chitosan composite film based biosensor for the sensitive and selective determination of dopamine. *Analyst*, 2013, 138: 5417–5423
41 Qu SN, Wang XY, Lu QP, Liu XY, Wang LJ. A biocompatible fluorescent ink based on water-soluble luminescent carbon nanodots. *Angew Chem Int Edit*, 2012, 51: 12215–12218
42 Liu Y, Liu CY, Zhang ZY. Graphitized carbon dots emitting strong green photoluminescence. *J Mater Chem C*, 2013, 1: 4902–4907
43 Ding CQ,Zhu AW, Tian Y. Functional surface engineering of C-dots for fluorescent biosensing and *in vivo* bioimaging. *Acc Chem Res*, 2014, 47: 20–30
44 Zhu H, Wang XL, Li YL, Wang ZJ, Yang F, Yang XR. Microwave synthesis of fluorescent carbon nanoparticles with electrochemiluminescence properties. *Chem Commun*, 2009: 5118–5120
45 Zhou JG, Booker C, Li RY, Zhou XT, Sham TK, Sun XL, Ding ZF. An electrochemical avenue to blue luminescent nanocrystals from multiwalled carbon nanotubes (MWCNTs). *J Am Chem Soc*, 2007, 129: 744–745
46 Zhao QL, Zhang ZL, Huang BH, Peng J, Zhang M, Pang DW. Facile preparation of low cytotoxicity fluorescent carbon nanocrystals by electrooxidation of graphite. *Chem Commun*, 2008: 5116–5118
47 Vinci JC, Ferrer IM, Seedhouse SJ, Bourdon AK, Reynard JM, Foster BA, Bright FV, Colon LA. Hidden properties of carbon dots revealed after hplc fractionation. *J Phys Chem Lett*, 2013, 4: 239–243
48 Hilderbrand SA, Weissleder R. Near-infrared fluorescence: application to *in vivo* molecular imaging. *Curr Opin Chem Biol*, 2010, 14: 71–79
49 Li HT, He XD, Liu Y, Huang H, Lian SY, Lee ST, Kang ZH. One-step ultrasonic synthesis of water-soluble carbon nanoparticles with excellent photoluminescent properties. *Carbon*, 2011, 49: 605–609
50 Li HT, Ming H, Liu Y, Yu H, He XD, Huang H, Pan KM, Kang ZH, Lee ST. Fluorescent carbon nanoparticles: electrochemical synthesis and their pH sensitive photoluminescence properties. *New J Chem*, 2011, 35: 2666–2670
51 Deng YH, Zhao DX, Chen X, Wang F, Song H, Shen DZ. Long lifetime pure organic phosphorescence based on water soluble carbon dots. *Chem Commun*, 2013, 49: 5751–5753
52 Zhu S, Meng Q, Wang L, Zhang J, Song Y, Jin H, Zhang K, Sun H, Wang H, Yang B. Highly photoluminescent carbon dots for multicolor patterning, sensors, and bioimaging. *Angew Chem Int Edit*, 2013, 52: 3953–3957
53 Anilkumar P, Wang X, Cao L, Sahu S, Liu JH, Wang P, Korch K, Tackett KN, Parenzan A, Sun YP. Toward quantitatively fluorescent carbon-based "quantum" dots. *Nanoscale*, 2011, 3: 2023–2027
54 Hsu PC, Chang HT. Synthesis of high-quality carbon nanodots from hydrophilic compounds: role of functional groups. *Chem Commun*, 2012, 48: 3984–3986
55 Jaiswal A, Ghosh SS, Chattopadhyay A. One step synthesis of c-dots by microwave mediated caramelization of poly(ethylene glycol). *Chem Commun*, 2012, 48: 407–409
56 Jia XF, Li J, Wang EK. One-pot green synthesis of optically pH-sensitive carbon dots with upconversion luminescence. *Nanoscale*, 2012, 4: 5572–5575
57 Hu SL, Niu KY, Sun J, Yang J, Zhao NQ, Du XW. One-step synthesis of fluorescent carbon nanoparticles by laser irradiation. *J Mater Chem*, 2009, 19: 484–488
58 Song YC, Feng D, Shi W, Li XH, Ma HM. Parallel comparative studies on the toxic effects of unmodified cdte quantum dots, gold nanoparticles, and carbon nanodots on live cells as well as green gram sprouts. *Talanta*, 2013, 116: 237–244
59 Wang K, Gao ZC, Gao G, Wo Y, Wang YX, Shen GX, Cui DX. Systematic safety evaluation on photoluminescent carbon dots.

Nanoscale Res Lett, 2013, 8: 122
60 Huang X, Zhang F, Zhu L, Choi KY, Guo N, Guo J, Tackett K, Anilkumar P, Liu G, Quan Q, Choi HS, Niu G, Sun YP, Lee S, Chen X. Effect of injection routes on the biodistribution, clearance, and tumor uptake of carbon dots. *ACS Nano*, 2013, 7: 5684–5693
61 Wang F, Xie Z, Zhang H, Liu CY, Zhang YG. Highly luminescent organosilane-functionalized carbon dots. *Adv Funct Mater*, 2011, 21: 1027–1031
62 Yang ST, Wang X, Wang HF, Lu FS, Luo PJG, Cao L, Meziani MJ, Liu JH, Liu YF, Chen M, Huang YP, Sun YP. Carbon dots as nontoxic and high-performance fluorescence imaging agents. *J Phys Chem C*, 2009, 113: 18110–18114
63 Zhang P, Yang JH, Li WC, Wang W, Liu CJ, Griffith M, Liu WG. Cationic polymer brush grafted-nanodiamond via atom transfer radical polymerization for enhanced gene delivery and bioimaging. *J Mater Chem*, 2011, 21: 7755–7764
64 Zhang XY, Wang SQ, Zhu CY, Liu MY, Ji Y, Feng L, Tao L, Wei Y. Carbon-dots derived from nanodiamond: photoluminescence tunable nanoparticles for cell imaging. *J Colloid Interf Sci*, 2013, 397: 39–44
65 Wei JM, Shen JM, Zhang X, Guo SK, Pan JQ, Hou XG, Zhang HB, Wang L, Feng BX. Simple one-step synthesis of water-soluble fluorescent carbon dots derived from paper ash. *RSC Adv*, 2013, 3: 13119–13122
66 Xu Y, Wu M, Liu Y, Feng XZ, Yin XB, He XW, Zhang YK. Nitrogen-doped carbon dots: a facile and general preparation method, photoluminescence investigation, and imaging applications. *Chem-Eur J*, 2013, 19: 2276–2283
67 Hsu PC, Shih ZY, Lee CH, Chang HT. Synthesis and analytical applications of photoluminescent carbon nanodots. *Green Chemistry*, 2012, 14: 917–920
68 Liu RL, Wu DQ, Liu SH, Koynov K, Knoll W, Li Q. An aqueous route to multicolor photoluminescent carbon dots using silica spheres as carriers. *Angew Chem Int Ed*, 2009, 48: 4598–4601
69 Zhu SJ, Zhang JH, Qiao CY, Tang SJ, Li YF, Yuan WJ, Li B, Tian L, Liu F, Hu R, Gao HN, Wei HT, Zhang H, Sun HC, Yang B. Strongly green-photoluminescent graphene quantum dots for bioimaging applications. *Chem Commun*, 2011, 47: 6858–6860
70 Yang YH, Cui JH, Zheng MT, Hu CF, Tan SZ, Xiao Y, Yang Q, Liu YL. One-step synthesis of amino-functionalized fluorescent carbon nanoparticles by hydrothermal carbonization of chitosan. *Chem Commun*, 2012, 48: 380–382
71 Chandra S, Das P, Bag S, Laha D, Pramanik P. Synthesis, functionalization and bioimaging applications of highly fluorescent carbon nanoparticles. *Nanoscale*, 2011, 3: 1533–1540
72 Goh EJ, Kim KS, Kim YR, Jung HS, Beack S, Kong WH, Scarcelli G, Yun SH, Hahn SK. Bioimaging of hyaluronic acid derivatives using nanosized carbon dots. *Biomacromolecules*, 2012, 13: 2554–2561
73 Dong W, Dong Y, Wang Y, Zhou S, Ge X, Sui L, Wang J. Labeling of human hepatocellular carcinoma cells by hexamethylene diamine modified fluorescent carbon dots. *Spectrochimica Acta Part A,* 2013, 116C: 209–213
74 Wang XH, Qu KG, Xu BL, Ren JS, Qu XG. Microwave assisted one-step green synthesis of cell-permeable multicolor photoluminescent carbon dots without surface passivation reagents. *J Mater Chem*, 2011, 21: 2445–2450
75 Choi HS, Liu W, Misra P, Tanaka E, Zimmer JP, Ipe BI, Bawendi MG, Frangioni JV. Renal clearance of quantum dots. *Nat Biotechnol*, 2007, 25: 1165–1170
76 Li N, Liang XF, Wang LL, Li ZH, Li PY, Zhu YH, Song J. Biodistribution study of carbogenic dots in cells and in vivo for optical imaging. *J Nanopart Res*, 2012, 14: 1177
77 Goncalves HMR, Duarte AJ, da Silva JCGE. Optical fiber sensor for Hg(II) based on carbon dots. *Biosens Bioelectron*, 2010, 26: 1302–1306
78 Zong J, Zhu YH, Yang XL, Shen JH, Li CZ. Synthesis of photoluminescent carbogenic dots using mesoporous silica spheres as nanoreactors. *Chem Commun*, 2011, 47: 764–766
79 Salinas-Castillo A, Ariza-Avidad M, Pritz C, Camprubi-Robles M, Fernandez B, Ruedas-Rama MJ, Megia-Fernandez A, Lapresta-Fernandez A, Santoyo-Gonzalez F, Schrott-Fischer A, Capitan-Vallvey LF. Carbon dots for copper detection with down and upconversion fluorescent properties as excitation sources. *Chem Commun*, 2013, 49: 1103–1105
80 Cao L, Wang X, Meziani MJ, Lu FS, Wang HF, Luo PJG, Lin Y, Harruff BA, Veca LM, Murray D, Xie SY, Sun YP. Carbon dots for multiphoton bioimaging. *J Am Chem Soc*, 2007, 129: 11318–11319
81 Zhu SJ, Zhang JH, Liu X, Li B, Wang XF, Tang SJ, Meng QN, Li YF, Shi C, Hu R, Yang B. Graphene quantum dots with controllable surface oxidation, tunable fluorescence and up-conversion emission. *RSC Adv*, 2012, 2: 2717–2720
82 Shen JH, Zhu YH, Chen C, Yang XL, Li CZ. Facile preparation and upconversion luminescence of graphene quantum dots. *Chem Commun*, 2011, 47: 2580–2582
83 Zhu AW, Qu Q, Shao XL, Kong B, Tian Y. Carbon-dot-based dual-emission nanohybrid produces a ratiometric fluorescent sensor for *in vivo* imaging of cellular copper ions. *Angew Chem Int Ed*, 2012, 51: 7185–7189
84 Kong B, Zhu AW, Ding CQ, Zhao XM, Li B, Tian Y. Carbon dot-based inorganic-organic nanosystem for two-photon imaging and biosensing of pH variation in living cells and tissues. *Adv Mater*, 2012, 24: 5844–5848
85 Li HL, Zhang YW, Wang L, Tian JQ, Sun XP. Nucleic acid detection using carbon nanoparticles as a fluorescent sensing platform. *Chem Commun*, 2011, 47: 961–963
86 Wang YH, Wang SM, Ge SG, Wang SW, Yan M, Zang DJ, Yu JH. Facile and sensitive paper-based chemiluminescence DNA biosensor using carbon dots dotted nanoporous gold signal amplification label. *Anal Methods-Uk*, 2013, 5: 1328–1336
87 Subhabrata M, Krishnendu D, Prasanta KD. Label-free fluorimetric detection of histone using quaternized carbon dot-DNA nanobiohybrid. *Chem Comm*, 2013, 49, 8851–8853
88 Zhang L, Cui P, Zhang BC, Gao F. Aptamer-based turn-on detection of thrombin in biological fluids based on efficient phosphorescence energy transfer from Mn-doped ZnS quantum dots to carbon nanodots. *Chem Eur J*, 2013, 19: 9242–9250
89 Yu CM, Li XZ, Zeng F, Zheng FY, Wu SZ. Carbon-dot-based ratiometric fluorescent sensor for detecting hydrogen sulfide in aqueous media and inside live cells. *Chem Commun*, 2013, 49: 403–405
90 Yu CM, Wu YL, Zeng F, Wu SZ. A fluorescent ratiometric nanosensor for detecting no in aqueous media and imaging exogenous and endogenous no in live cells. *J Mater Chem B*, 2013, 1: 4152–4159
91 Fangkai Du YM, Fang Zeng, Changming Yu, Shuizhu Wu. A targeted and fret-based ratiometric fluorescent nanoprobe for imaging mitochondrial hydrogen peroxide in living cells. *Small*, 2013, 9: DOI: 10.1002/smll.201302036
92 Lin Z, Xue W, Chen H, Lin JM. Classical oxidant induced chemiluminescence of fluorescent carbon dots. *Chem Commun*, 2012, 48: 1051–1053
93 Xue W, Lin Z, Chen H, Lu C, Lin JM. Enhancement of ultraweak chemiluminescence from reaction of hydrogen peroxide and bisulfite by water-soluble carbon nanodots. *J Phys Chem C*, 2011, 115: 21707–21714
94 Zhao LX, Di F, Wang DB, Guo LH, Yang Y, Wan B, Zhang H. Chemiluminescence of carbon dots under strong alkaline solutions: a novel insight into carbon dot optical properties. *Nanoscale*, 2013, 5: 2655–2658

95 Shi JX, Lu C, Yan D, Ma LN. High selectivity sensing of cobalt in HepG2 cells based on necklace model microenvironment-modulated carbon dot-improved chemiluminescence in fenton-like system. *Biosens Bioelectron*, 2013, 45: 58–64
96 Zheng LY, Chi YW, Dong YQ, Lin JP, Wang BB. Electro-chemiluminescence of water-soluble carbon nanocrystals released electrochemically from graphite. *J Am Chem Soc*, 2009, 131: 4564–4565
97 Zhang M, Liu H, Chen L, Yan M, Ge L, Ge S, Yu J. A disposable electrochemiluminescence device for ultrasensitive monitoring of k562 leukemia cells based on aptamers and ZnO@carbon quantum dots. *Biosens Bioelectron*, 2013, 49: 79–85
98 Li Q, Ohulchanskyy TY, Liu RL, Koynov K, Wu DQ, Best A, Kumar R, Bonoiu A, Prasad PN. Photoluminescent carbon dots as biocompatible nanoprobes for targeting cancer cells *in vitro*. *J Phys Chem C*, 2010, 114: 12062–12068
99 Qin XY, Asiri AM, Alamry KA, Al-Youbi AO, Sun XP. Carbon nitride dots can serve as an effective stabilizing agent for reduced graphene oxide and help in subsequent assembly with glucose oxidase into hybrids for glucose detection application. *Electrochim Acta*, 2013, 95: 260–267
100 Song YC, Shi W, Chen W, Li XH, Ma HM. Fluorescent carbon nanodots conjugated with folic acid for distinguishing folate-receptor-positive cancer cells from normal cells. *J Mater Chem*, 2012, 22: 12568–12573
101 Qi Gao Q, Han JM, Ma ZF. Polyamidoamine dendrimers-capped carbon dots/au nano crystal nano composites and its application for electrochemical immunosensor. *Biosens Bioelectron*, 2013, 49: 323–328
102 Ludan Wu ML, Meng Zhang, Mei Yan, Shenguang Ge, Jinghua Yu. Ultra sensitive electro chemiluminescence immunosensor for tumor marker detection based on nanoporous sliver@carbon dots as labels. *Sensors Actuat B-Chem*, 2013, 186: 761–767
103 Huang P, Lin J, Wang XS, Wang Z, Zhang CL, He M, Wang K, Chen F, Li ZM, Shen GX, Cui DX, Chen XY. Light-triggered theranostics based on photosensitizer-conjugated carbon dots for simultaneous enhanced-fluorescence imaging and photodynamic therapy. *Adv Mater*, 2012, 24: 5104–5110
104 Vinit K, Giuseppe T, Flavio R. Fluorescent carbon nanoparticles in medicine for cancer therapy. *ACS Med Chem Lett*, 2013, 4: 1012–1013
105 Zhou L, Li ZH, Liu Z, Ren JS, Qu XG. Luminescent carbon dot-gated nanovehicles for ph-triggered intracellular controlled release and imaging. *Langmuir*, 2013, 29: 6396–6403
106 Chen H, Zhen Z, Tang W, Todd T, Chuang YJ, Wang L, Pan Z, Xie J. Label-free luminescent mesoporous silica nanoparticles for imaging and drug delivery. *Theranostics*, 2013, 3: 650–657
107 Wang QL, Huang XX, Long YJ, Wang XL, Zhang HJ, Zhu R, Liang LP, Teng P, Zheng HZ. Hollow luminescent carbon dots for drug delivery. *Carbon*, 2013, 59: 192–199
108 Kim J, Park J, Kim H, Singha K, Kim WJ. Transfection and intracellular trafficking properties of carbon dot-gold nanoparticle molecular assembly conjugated with PEI-PDNA. *Biomaterials*, 2013, 34: 7168–7180